Structural Analysis of the IL-15/IL-15Rα Complex

Interleukin (IL)-15 and IL-2, which promote the survival of memory CD8$^+$ T cells and regulatory T cells, respectively, bind receptor complexes that share β- and γ-signaling subunits. Receptor specificity is provided by unique, non-signaling α subunits. Whereas IL-2Rα is co-expressed *in cis* with the β- and γ-subunits on T and B cells, IL-15Rα is expressed *in trans* on antigen-presenting cells. The crystal structure of the human IL-15/IL-15Rα complex solved at 1.85 Å provides new insights into the molecular basis for the specificity of cytokine recognition, and highlights the important role of water in generating this very high-affinity complex.

Interleukin (IL)-15 and IL-2, which promote the survival of memory CD8$^+$ T cells and regulatory T cells, respectively, bind receptor complexes that share β- and γ -signaling subunits. In addition, IL-15 and IL-2 have private receptors IL-15 receptor (R) α and IL-2Rα, respectively. Whereas IL-2Rα is co-expressed *in cis* with the β- and γ-subunits on T and B cells, IL-15 is *trans*-presented by IL-15Rα-expressed on antigen presenting cells to T cells expressing IL-2Rβ and γc. In contrast to the apparent *in cis* autocrine signaling triggered by IL-2, IL-15-dependent signaling is likely to be influenced by cell-cell contact. To reveal the molecular basis of recognition between IL-15 and IL-15Rα, we solved the crystal structure of the human IL-15/IL-15Rα complex [1].

IL-15 and the extracellular region of IL-15Rα were both expressed in *E. coli*, then purified as a complex. Initial crystallization screening was performed using the TOPAZ system (Fluidigm). The IL-15/IL15Rα complex crystals for structure analysis were then grown using the sitting-drop vapor-diffusion method. The complex crystallized in two different forms under the same conditions. One crystal form belongs to space group $P2_12_12$ with cell dimensions of a=78.4Å, b=120.0Å, and c=49.5Å. The other crystal form belongs to space group $P2_12_12_1$ with cell dimensions of a=81.8Å, b=127.0Å, and c=191.3Å. The $P2_12_12$ native and K_2PtCl_6 derivative crystals and $P2_12_12_1$ native crystals were transferred to mother liquor containing 10% v/v glycerol for data collection at AR-NW12A. The complex structure from the $P2_12_12$ crystals was initially determined at 2.9 Å resolution with the K_2PtCl_6 derivative data using the single anomalous dispersion method and the program Phenix. The phases were then extended to 1.85 Å using the $P2_12_12$ native data. The structure was manually built using the program Coot, and refined using the programs CNS and Refmac. The $P2_12_12_1$ structure was solved by molecular replacement using the program COMO and the refined $P2_12_12$ crystal structure. The $P2_12_12_1$ crystal structure was refined at 2.0 Å resolution using the programs CNS and Refmac.

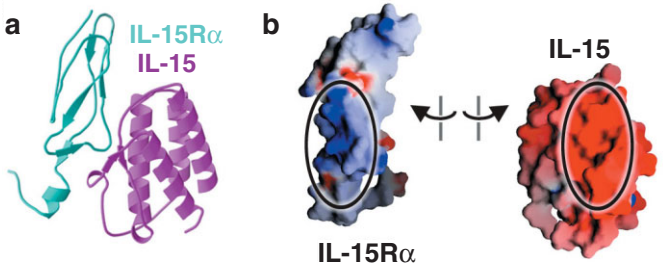

Figure 1
Structure of the human IL-15/IL-15Rα complex. (a) Ribbon representation of the IL-15/IL-15Rα complex. IL-15 and IL-15Rα are shown in magenta and cyan, respectively. (b) Open-book style representation of the binding faces represented as GRASP surfaces of IL-15Rα (left) and IL-15 (right), shown with blue representing positive charge and red negative charge contoured at ±10.0 kT. The approximate receptor subunit binding surfaces are indicated with ovals.

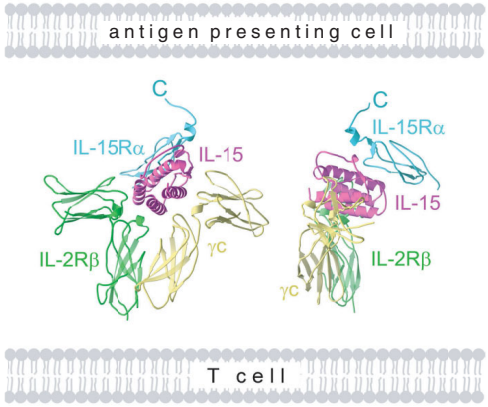

Figure 2
Two orthogonal views of the IL-15/IL-15Rα complex modeled with IL-2Rβ and γc. IL-15, IL-15Rα, IL-2Rβ and γc are shown in magenta, cyan, green and yellow, respectively.

In the IL-15/IL-15Rα complex, IL-15Rα uses the C-terminal half of its sushi domain to perch in a parallel orientation on the side and toward the top of IL-15 (Fig. 1a). Overall, the structure of the IL-15/IL-15Rα complex was extremely similar, with an rmsd of 1.96 Å for 126 residues to the complex formed by IL-2Rα and IL-2 in the IL-2 signaling complex solved to 2.3 Å resolution [2].

The binding of IL-15 to IL-15Rα is of extremely high (picomolar) affinity. However, the IL-15/IL-15Rα interaction conspicuously lacked a binding 'hot-spot', and binding was instead mediated by positively (IL-15Rα) and negatively (IL-15) charged residues (Fig. 1b). The interaction was further stabilized by an extensive water-mediated hydrogen bonding network between IL-15 and IL-15Rα. The lower electrostatic and geometric complementarity, together with the lack of an extensive water-mediated hydrogen bonding network in the IL-2/IL-2Rα complex [2], may account for the three orders of magnitude difference in the affinities of the IL-15/IL-15Rα and IL-2/IL-2Rα interactions. Superposition of IL-15 in the IL-15Rα complex with IL-2 in the complex with IL-2Rα, IL-2Rβ and γc [2] allows a plausible model of the quaternary IL-15 signaling complex to be assembled (Fig. 2). Importantly, the C-termini of IL-15Rα and IL-2Rα occupy similar membrane-distal positions with respect to the membrane anchorage of IL-2Rβ and γc, consistent with the possibility that IL-15 and IL-2 may be presented *in trans* to IL-2Rβ and γc expressing cells by IL-15Rα and IL-2Rα, respectively.

REFERENCES

[1] M. Chirifu, C. Hayashi, T. Nakamura, S. Toma, T. Shuto, H. Kai, Y. Yamagata, S.J. Davis and S. Ikemizu, *Nature Immunol.*, **8** (2007) 1001.
[2] X. Wang, M. Rickert and K.C. Garcia, *Science*, **310** (2005) 1159.

BEAMLINE

AR-NW12A

M. Chirifu[1], C. Hayashi[1], T. Nakamura[1], S. Toma[2], T. Shuto[1], H. Kai[1], Y. Yamagata[1], S.J. Davis[3] and S. Ikemizu[1] ([1]Kumamoto Univ., [2]The Univ. of Tokyo, [3]The Univ. of Oxford)

Structural Study of [NiFe] Hydrogenase Maturation Proteins, HypC, HypD and HypE from *Thermococcus kodakaraensis* KOD1

The crystal structures of [NiFe] hydrogenase maturation proteins, HypC, HypD and HypE from *Thermococcus kodakaraensis* KOD1 have been determined by the use of synchrotron radiation at the Photon Factory. The maturation of [NiFe] hydrogenases, including the insertion and cyanation of the iron center, requires several maturation proteins. Our results reveal the structural features of each protein, the functional roles of conserved motifs of the proteins, and give insights into the maturation process of [NiFe] hydrogenases. In the structure of HypD, the probable iron-binding active sites for cyanation are found, and the [4Fe-4S] cluster environment is shown to be quite similar to that of ferredoxin:thioredoxin reductase (FTR). These results suggest a cyanation reaction mechanism via unique thiol redox signaling in the HypCDE complex.

[NiFe] hydrogenases catalyze the reversible reaction to form molecular hydrogen in a variety of microorganisms. The core enzyme of the [NiFe] hydrogenases carries a $NiFe(CO)(CN)_2$ metal center at the active site. The synthesis of this metal center is a complex process, which requires the specific maturation proteins HypA, HypB, HypC, HypD, HypE, and HypF [1]. HypA and HypB are involved in the insertion of the Ni atom into the precursor large subunit, as [NiFe] hydrogenases are composed of large and small subunits. HypE and HypF are involved in the synthesis of the cyanide ligand attached to the active site Fe atom. HypF catalyzes the transfer of the carbamoyl group from carbamoylphosphate to the C-terminal cysteine residue of HypE coupled with the conversion of ATP to AMP and PPi. An ATP-dependent dehydration by HypE converts HypE-carboxamide to HypE-thiocyanate. HypC and HypD form a complex that is presumably involved in the insertion of the Fe atom coordinated by diatomic ligands. The HypCD complex receives the cyanide ligand from HypE-thiocyanate and is assumed to insert the Fe atom to the precursor of the large subunit of [NiFe] hydrogenases. However, the mechanism of the CN transfer to the iron atom in the ternary complex remains unclear. In order to gain insight into the mechanism of the cyanation reaction, we have determined the crystal structures of HypC, HypD, and HypE from *Thermococcus kodakaraensis* KOD1 at 1.8Å, 2.07Å, and 1.55Å resolution , respectively [2]. Data collection at the Photon Factory was performed at the AR-NW12.

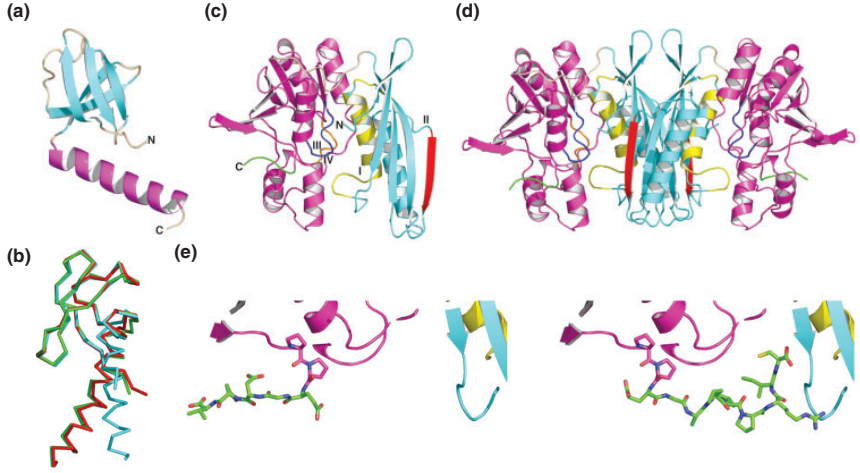

Figure 1
Crystal structures of HypC and HypE
(a) Overall structure of HypC in a ribbon representation. The OB fold domain is shown in cyan; the C-terminal α helix is shown in pink. (b) A superposition of the Cα backbone of the three HypC molecules in the asymmetric unit. (c) Overall structure of HypE. The two α/β domains A and B, and the C-terminal tail are shown in cyan, pink, and green, respectively. The conserved motifs, I, II, III, and IV are colored yellow, red, blue, and orange, respectively. (d) Overall structure of the HypE dimer. (e) Conformations of the C-terminal tail of HypE in the absence of ATP (left panel) and in the presence of ATP (right panel). In the latter (right panel), the electron density of ATP was not observed.

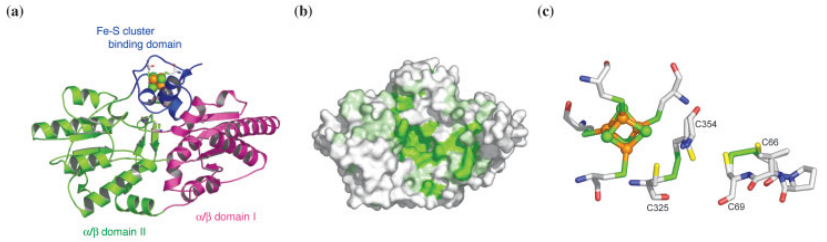

Figure 2
Crystal structure of HypD
(a) Ribbon representation of the overall structure. The two α/β domains I and II, and the Fe-S cluster binding domain are shown in magenta, green, and blue, respectively. Cysteine residues and the [4Fe-4S] cluster are represented by a stick-and-sphere model. (b) Surface representation. Identical and conserved residues among the HypD proteins are colored in green and light green, respectively. The orientation is identical to that in Fig. 2a. (c) Redox cascade between the [4Fe-4S] cluster and two disulfide bonds. Sulfur atoms in the dithiol form of cysteine residues are shown in yellow.

The overall structure of HypC consists of an OB fold-like β-barrel domain and a C-terminal α helix (Fig.1a). Three HypC monomers exist in the asymmetric unit, and their comparison has shown that the arrangement of the OB-fold domain and the C-terminal α helix differs between monomers (Fig. 1b), suggesting that the C-terminal α helix is very flexible.

The monomer structure of HypE consists of two α/β domains (domains A and B) and a C-terminal tail (Fig. 1c). HypE forms a homodimer, in which the β sheet of domain A from each monomer forms a pseudo ten-stranded β-barrel (Fig. 1d). This structure is similar to that of other PurM proteins, whose members are characterized by a common motif for ATP hydrolysis. The C-terminal tail of HypE is outwardly extended in the absence of ATP (Fig. 1e, left panel). On the other hand, in the presence of ATP, this C-terminal tail takes an inward conformation (Fig. 1e, right panel), although the electron density of ATP was not observed in this conformation. This feature shows an ATP-dependent dynamic equilibrium between the outward and inward conformations.

The overall architecture of HypD consists of three domains: an α/β domain I, an α/β domain II, and an Fe-S cluster binding domain with [4Fe-4S], and is not similar to any other known structures (Fig. 2a). The three domains form a cleft at the center of the molecule. Mapping of conserved residues on the molecular surface has shown that the residues around the center cleft are highly conserved (Fig. 2b). The highly conserved center cleft probably plays an important role in the activities of HypD. The crystal structure of HypD reveals that the [4Fe-4S] cluster environment of HypD is quite similar to that of ferredoxin:thioredoxin reductase (FTR), suggesting the existence of a redox cascade between the 4Fe-4S cluster and two disulfide bonds (Fig. 2c). The FTR-like redox cascade in HypD implies that the cyanation reaction is catalyzed by unique thiol redox signaling in the HypCDE complex.

REFERENCES

[1] A. Böck, P.W. King, M. Blokesch and M.C. Posewitz, *Adv. Microb. Physiol.*, **51** (2006) 1.
[2] S. Watanabe, R. Matsumi, T. Arai, H. Atomi, T. Imanaka and K. Miki, *Mol. Cell*, **27** (2007) 29.

BEAMLINE

AR-NW12

S. Watanabe[1] and K. Miki[1,2] ([1]Kyoto Univ. [2]RIKEN/SPring-8)

Protein-based Peptide-bond Formation by Aminoacyl-tRNA Protein Transferase

Bacterial leucyl/phenylalanyl-tRNA protein transferase (LF-transferase) catalyzes peptide-bond formation by using Leu-tRNA^{Leu} (or Phe-tRNA^{Phe}) and a protein bearing an N-terminal Arg (or Lys) as donor and acceptor substrates, respectively. Complex structures of LF-transferase and a phenylalanyl-tRNA^{Phe} analog, phenylalanyl adenosine (rAPhe), with and without a short peptide bearing an N-terminal Arg, have been determined. Combining the two separate structures into one structure and structural based mutation studies have revealed the catalytic mechanism for peptide bond formation by LF-transferase. The peptide bond formation by LF-transferase is similar to the reverse reaction of the acylation step observed in the peptide hydrolysis reaction by serine proteases.

Regulated degradation of intracellular proteins is essential for the control of post-translational gene expression in all organisms. The N-end rule, one of the vital proteolytic pathways, controls the half-life of proteins by destroying them according to their N-terminal amino acid residue, and is involved in higher cellular functions.

In the degradation of proteins governed by the N-end rule in both eubacteria and eukarya, an aminoacyl-tRNA protein transferase is involved in the conjugation of a primary destabilizing amino acid to the N-terminal residue of proteins, using cognate aminoacyl-tRNAs as amino acid donor substrates. The aminoacyl-tRNA protein transferase transfers the amino acid from the aminoacyl-tRNA to the amino group of the protein, facilitating peptide bond formation. However, the catalytic mechanism of peptide bond formation by the aminoacyl-RNA protein transferase has remained obscure for more than thirty years.

Bacterial leucyl/phenylalanyl-tRNA protein transferase (LF-transferase) catalyzes peptide-bond formation by using Leu-tRNA^{Leu} (or Phe-tRNA^{Phe}) and a protein bearing N-terminal Arg (or Lys) as donor and acceptor substrates, respectively. In this report, the complexes of LF-transferase and a phenylalanyl-tRNA^{Phe} analog, phenylalanyl adenosine (rAPhe), with and without a short peptide bearing N-terminal Arg (α-casein fragment: Arg-Tyr-Leu-Gly), were crystallized, and diffraction data were recorded at beamlines AR-NW12A, BL-5A or BL-17A. All of the data were processed using the HKL2000 program, and their structures were solved at resolutions of 2.4–2.85 Å. Combining the two separate structures we determined, one with rA-Phe and one with a product peptide (Phe-Arg-Tyr-Leu-Gly), into one structure has revealed the mechanism for the substrate specificity and the catalytic reaction of peptide bond formation by LF-transferase. This was confirmed by structure-based mutation studies [1].

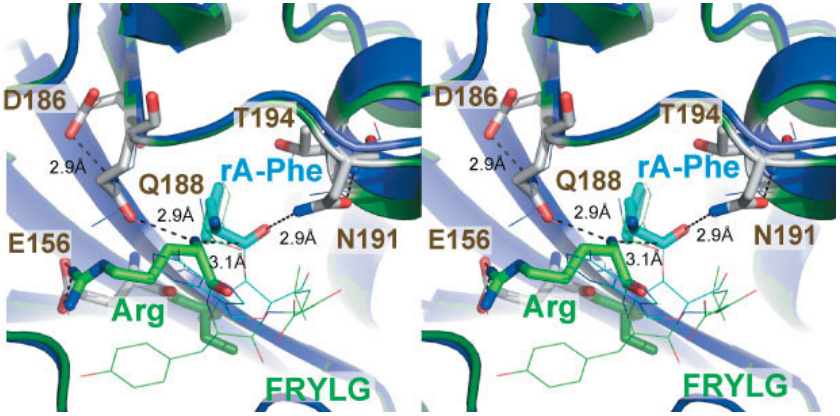

Figure 1
A stereo-view of superposition of the two complexes. The complex with rA-Phe and that with the product peptide (the amino acid sequence is FRYLG, where F is transferred to the N-terminal R of α-casein fragment RYLG) are colored blue and dark green, respectively. The benzyl group of rA-Phe and the Arg in the product peptide are colored cyan and green, respectively, and are shown in stick models.

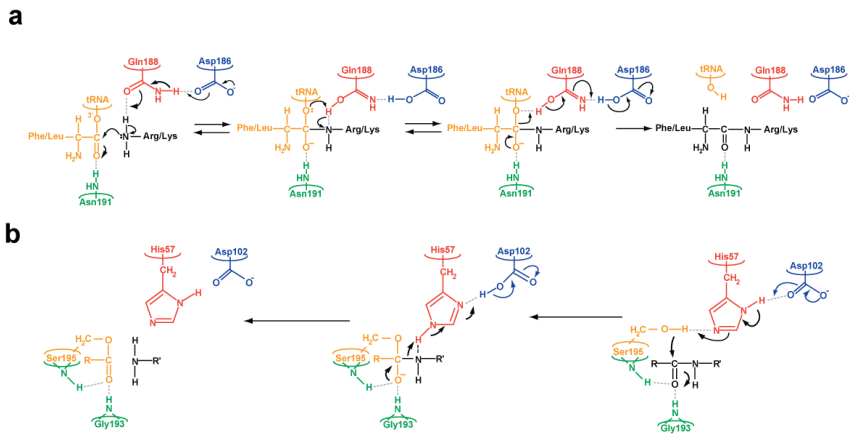

Figure 2
Comparison of the catalytic mechanism for peptide bond formation by LF-transferase (a) with the reverse reaction of the acylation step during peptide hydrolysis by chymotrypsin (b).

The electron relay from Asp^{186} to Gln^{188} helps Gln^{188} to abstract a proton from the alpha-amino group of the N-terminal Arg of the acceptor peptide. This generates the attacking nucleophile for the carbonyl carbon of the aminoacyl bond of the aminoacyl-tRNA, thus facilitating peptide bond formation (Fig. 1). The protein-based general base-catalyzed mechanism, involving the catalytic dyad of Gln^{188} and Asp^{186}, for peptide bond formation by LF-transferase is similar to the reverse reaction of the acylation step observed in the peptide hydrolysis reaction by serine proteases (Fig. 2). The catalytic mechanism by LF-transferase uncovered here is different from that on the ribosome, where the substrate-associated proton shuttle, in cooperation with the neighboring rRNA and water molecules, is the underlying mechanism of peptide bond formation.

The chemical reaction of peptide-bond formation by LF-transferase is the same as that of protein synthesis on the ribosome. Proteins bearing N-terminal Arg (or Lys) and Phe-tRNA^{Phe} (or Leu-tRNA^{Leu}) correspond to the A-site and P-site tRNAs in peptide bond formation on the ribosome, respectively. However, the catalytic mechanism for peptide bond formation by LF-transferase implies that the reaction involves chemical catalysis by the electron relay from Asp^{186} to Gln^{188}. Therefore, the catalytic mechanisms for peptide bond formation by LF-transferase and by the ribosome are fundamentally different, and LF-transferase utilizes the protein-based mechanism for peptide bond formation. This not only uncovers the anticipated features of the peptide-bond formation by protein, but could also be expanded to molecular evolution of the catalytic mechanism of protein synthesis in living organisms and could provide significant insight into the mechanism of protein synthesis on ribosome.

REFERENCE

[1] K. Watanabe, Y. Toh, K. Suto, Y. Shimizu, N. Oka, T. Wada and K. Tomita, *Nature,* **449** (2007) 867.

BEAMLINE

5A, 17A and AR-NW12A

K. Watanabe[1], Y. Toh[1], K. Tomita[1,2] ([1]AIST, [2]JST, PRESTO)

Structural Studies of RbfA and its Complex with the 30S Ribosomal Subunit Reveals How RbfA Helps Bacteria Survive under Cold-shock Conditions

In all living cells, protein biosynthesis takes place at the ribosome, a gigantic ribonucleoprotein complex. A bacterial cold-shock response protein, RbfA plays a critical role during the assembly of the ribosome small (30S) subunit. We have determined a crystal structure of *Thermus thermophilus* RbfA and a cryo-electron microscopic reconstruction of the RbfA-30S complex at resolutions of 1.84 Å and 12.5 Å, respectively. RbfA binds to functionally important regions of the 30S subunit, where RNA helices exhibit large-scale conformational changes. These results reveal that RbfA plays a dual role in the maturation of the 30S subunit as well as in cold-shock adaptation of cells.

The ribosome is a macromolecular machine composed of 65% ribosomal RNA (rRNA) and 35% ribosomal proteins (r-proteins), where messenger RNA (mRNA) is translated into proteins. Bacterial ribosomes consist of small (30S) and large (50S) subunits. In the 30S subunit, the genetic information of mRNA is decoded by transfer RNAs (tRNAs) that deliver amino acids to the ribosome. The 30S subunit comprises 21 r-proteins as well as 16S rRNA, which is firstly transcribed as a longer RNA, processed via 17S RNA by specific nucleases, and bound by r-proteins in acquisition of the three-dimensional structure. There also appear to be additional protein factors, the exact roles of which remain to be defined [1].

Ribosome binding factor A (RbfA) is known as a bacterial cold-shock response protein, and required for an efficient processing of rRNA during the assembly of the 30S subunit. RbfA is expressed constitutively under normal growth conditions; however, the expression level rapidly increases upon cold shock. The elevated levels of RbfA under cold-shock conditions are necessary to overcome the translational block at the reduced temperature, presumably by facilitating rapid maturation of the 30S subunits. We joined up with German and American scientists to investigate RbfA-ribosome interactions in order to understand the mechanism of this cold-shock response [2].

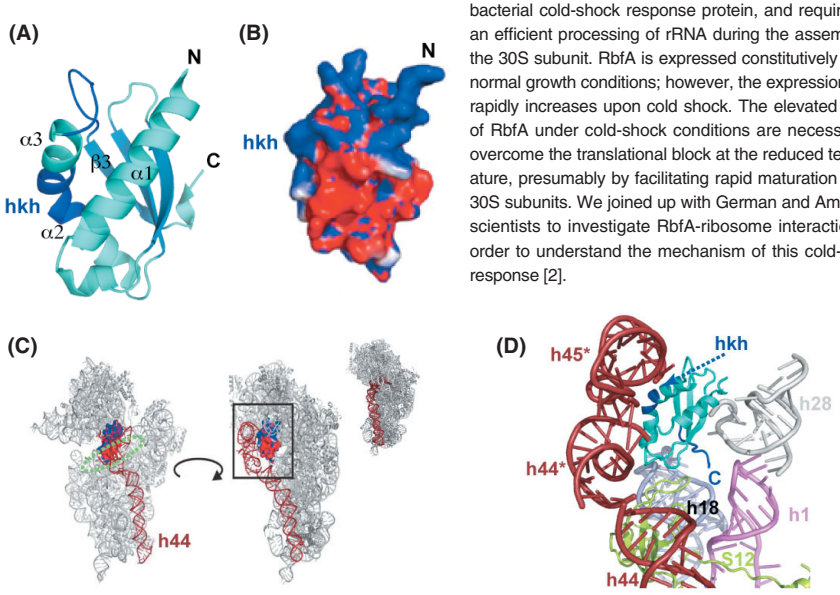

Figure 1
Dramatic conformational changes in the 30S subunit by the RbfA binding.
(A) The crystal structure of *T. thermophilus* RbfA. The RNA-binding helix-kink-helix motif (hkh) and a flexible loop between α3 and β3 are colored in blue. The N- and C-terminal ends are denoted by "N" and "C", respectively. (B) The electrostatic potential is mapped on the molecular surface of RbfA, viewed from the same angle as in (A). Negatively and positively charged regions are colored in red and blue, respectively. (C) Front (subunit interface) and side (rotated 30° counterclockwise) views of the RbfA-30S complex. The bound RbfA, depicted as in (B), occludes the binding sites of mRNA and tRNA (encircled by a green dotted line). Functionally important rRNA helices 44 and 45 (h44 and h45; brown) exhibit large-scale conformational changes. The 30S subunit alone (PDB: 2J00) is shown as thumbnail with the same angle and coloring as the right panel. (D) The strategic location of RbfA on the 30S subunit, and interaction of RbfA with multiple rRNA helices and r-proteins. RbfA binds behind relocated helices 44 and 45 (h44* and h45*; brown), such that the hkh motif (hkh; blue) faces the junction of h44 and h45. The C-terminal flexible tail (C; blue) extends deep into the 30S subunit and approaches helix1 (h1; pink) at the 5' end of the 16S rRNA. The other major contact sites are helices 18 and 28 (h28; gray and h18; light blue) and r-protein S12 (S12; light green).

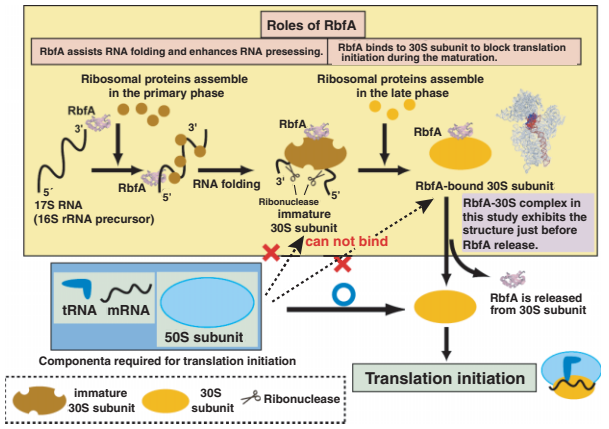

Figure 2
Roles of RbfA during the 30S subunit maturation.
17S RNA is produced as a precursor of 16S rRNA. At the initial phase of maturation, RbfA binds to the 17S RNA and helps h1 formation. Some ribosomal proteins also bind to specific binding sites of the 17S RNA, forming an immature 30S subunit. Subsequently, 5' and 3' extra sequences of the 17S RNA are processed by some ribonucleases, and RbfA remains bound on the immature 30S subunit for further maturation. The bound RbfA induces large-scale relocations of h44 and h45, thereby preventing the immature 30S subunit from binding with components essential for translation initiation, such as mRNA, tRNA, and the 50S subunit. Finally at the late maturation phase, RbfA is released as the remaining ribosomal proteins assemble into the immature 30S subunit, and the resultant mature 30S subunit is ready for translation initiation.

Firstly, we have determined a crystal structure of *T. thermophilus* RbfA, using diffraction data collected at the BL-5A. The structure represents a single KH-domain containing three α-helices (α1 to α3) and three β-strands (β1 to β3) with an αββααβ topology (Fig. 1(A)). The α2 and α3 helices are arranged to form a helix-kink-helix (hkh), known as an RNA-binding motif. Positively charged surfaces consist of the hkh motif, the loop between α3 and β3, and the N-terminal end (Fig. 1(B)), and the overall patterns of charge distribution among known RbfA structures are highly conserved, despite their low amino acid sequence identity (20%). Furthermore, significant conformational differences among the structures are found in these charged regions, suggesting that these regions possess functional importance due to the structural flexibility.

We subsequently obtained a cryo-electron microscopic (EM) reconstruction of the *T. thermophilus* RbfA-30S complex. A subtraction of the coordinates of the 30S subunit (PDB: 1J5E) from the cryo-EM map delineated the boundaries of extra density, which encloses a space (19,384 Å^3) much larger than that expected from the *T. thermophilus* RbfA structure (10,764 Å^3). By contouring to very high threshold values, only double-stranded RNA helices became visible, because they possess higher electron dense than protein. Our analysis shows that the extra density corresponds to the shifted helices h44 and h45 of 16S rRNA, and the bound RbfA protein (Fig. 1(C)). The hkh motif of RbfA faces the junction between h44 and h45, consistent with the charge distribution, whereas the flexible C-terminus of RbfA extends to h1 at the 5'-end of the 16S rRNA (Fig. 1(D)). It is notable that the RbfA binding causes a dramatic relocation of h44, a functionally important segment of the 16S rRNA that is directly involved in mRNA decoding, tRNA binding and association with the 50S subunit.

These results indicate that the RbfA binding helps the proper folding of the 30S subunit and prevent the immature subunit from association with components required for translation initiation (Fig. 2) Thus, RbfA confers a translational advantage to cells under cold-shock conditions where ribosome formation becomes inefficient.

REFERENCES

[1] D.N. Wilson and K.H. Nierhaus, *Crit. Rev. Biochem. Mol. Biol.*, **42** (2007) 187.
[2] P.P. Datta, D.N. Wilson, M. Kawazoe, N.K. Swami, T. Kaminishi, M.R. Sharma, T.M. Booth, C. Takemoto, P. Fucini, S. Yokoyama and R.K. Agrawal, *Mol. Cell*, **28** (2007) 434.

BEAMLINE

5A

C. Takemoto, M. Kawazoe, T. Kaminishi and S. Yokoyama (RIKEN)

The Structure and Function of Human Transportin 1

Transportin 1 (Trn1) is a transport receptor that transports substrates ("cargoes") from the cytoplasm to the nucleus. We have determined the crystal structures of human Trn1 in its substrate-free form, as well as in complex with three nuclear localization signals (NLSs). Our data revealed that (i) Trn1 has two NLS binding sites (A and B), and that the NLS interaction at site B controls the overall binding affinity for Trn1, (ii) Trn1 recognizes the NLSs at Site A followed by conformational change at Site B to interact with the NLSs, and (iii) a long flexible loop, characteristic of Trn1, interacts with Site B, thereby displacing the transport substrate in the nucleus.

The nuclear-cytoplasmic transport of macromolecules through nuclear pore complexes (NPCs) is mediated by transport receptors that are most commonly members of the importin-β family [1]. The transport receptors form complexes with their transport substrates through cognate nuclear localization signals (NLSs) for import substrates or nuclear export signals (NESs) for export substrates, and target their substrates to NPC components. Transportin 1 (Trn1) was first identified for the heterogeneous nuclear ribonucleoprotein A1 (hnRNP A1) [2]. Other substrates whose transport is also mediated by Trn1 have since emerged. The NLSs of these substrates have little sequence similarity, but recent mutational analyses have shown the importance of two successive proline and tyrosine residues (the PY motif) conserved in the NLSs of hnRNP D, TAP, JKTBP, hnRNP A1, and hnRNP M [2,3]. Here, we show the crystal structures of human Trn1 corresponding to Trn1 in a substrate-free form and bound to the following three NLS peptides which all have a PY motif: hnRNP D NLS (residues 332-355), TAP NLS (residues 53-82), and JKTBP NLS (residues 396-420), and propose a mechanism for NLS recognition and dissociation from Trn1 [4]. Diffraction data for Trn1 bound to TAP NLS were collected using an ADSC Quantum 210 CCD detector at beamline AR-NW12A, and those for NLS-free Trn1 and Trn1 bound to hnRNP D NLS and JKTBP NLS were collected at BL41-XU, SPring-8.

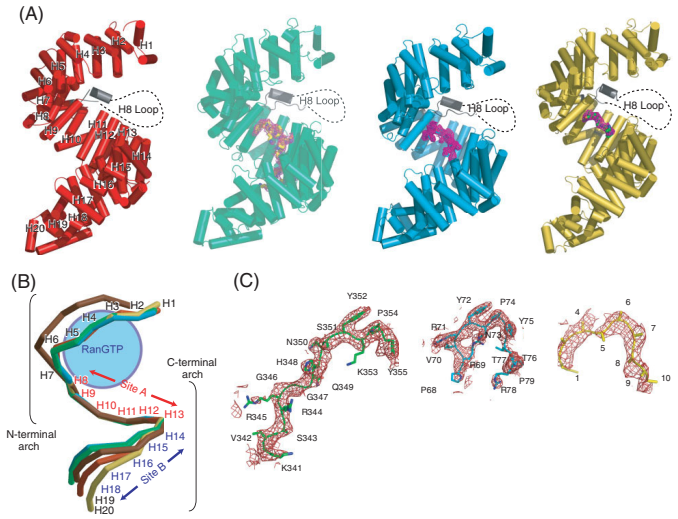

Figure 1
Structures of Trn1. (A) Overall structures of NLS-free Trn1 (red) and Trn1 bound to hnRNP D NLS (green), TAP NLS (blue), and JKTBP NLS (yellow), where α helices are represented as cylinders. The 20 consecutive HEAT repeats (H1-H20), each of which is composed of two antiparallel helices, are labeled on the NLS-free Trn1 structure. The H8 loop is shown as a black cylinder (α helix) and a black dotted line (disordered region). (B) Trn1 structure showing the conformational changes upon either RanGTP or NLS binding. The structures of NLS-free Trn1 (red), Trn1 bound to hnRNP D NLS (green), Trn1 bound to TAP NLS (blue), Trn1 bound to JKTBP NLS (yellow), and the Trn1-RanGTP complex (brown) are superimposed in the overlapping region of the N- and C-terminal arches (HEAT repeats 8-13). The 20 consecutive HEAT repeats in each Trn1 molecule are represented by straight lines. The structure of the Trn1-Ran complex was drawn using the refined coordinates deposited in the Protein Data Bank (accession code: 1QBK). (C) The CNS composite simulated annealing omit map of the NLS region bound to Trn1. The map was calculated with coefficient $2F_o - F_c$ and contoured at 1.0 σ. NLSs of hnRNP D, TAP, and JKTBP are shown as stick models colored green, blue, and yellow, respectively. For JKTBP NLS bound to Trn1, the electron density of JKTBP NLS is so weak that the side chains of the amino acid residues could not be assigned unambiguously.

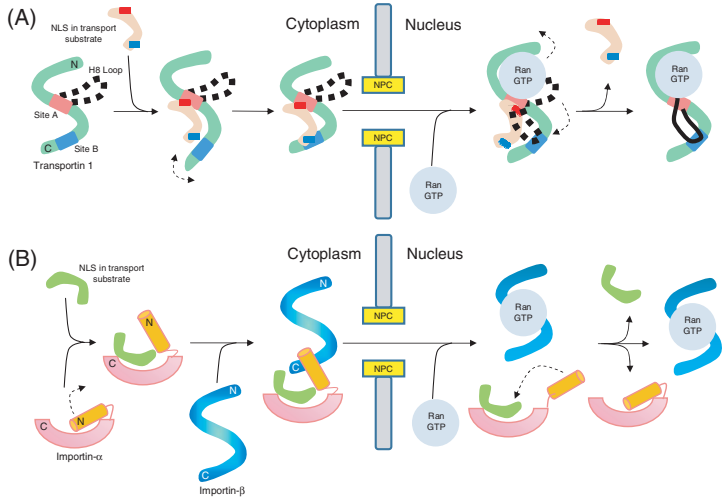

Figure 2
Proposed mechanisms for the nuclear import pathway mediated by Trn1 (A) and importin-β (B). NPC is the nuclear pore complex. The Trn1 and importin-β molecules are represented by S-like ribbons labeled with N- and C-termini. Red and blue rectangles on the NLS in (A) show the three consensus residues (red rectangle) and one hydrophobic residue (blue rectangle). The orange cylinder in (B) represents an α-helical domain of importin-α that interacts with importin-β.

Trn1 is a superhelical S-like molecule formed by two overlapping arches (the N- and C-terminal arches), and is constructed by the helical stacking of the 20 HEAT repeats (H1-H20) and a long disordered H8 loop (Fig. 1(A)). The structure of the N-terminal arch (HEAT repeats 1-13) is almost the same in the four Trn1 structures, whereas that of the C-terminal arch (HEAT repeats 8-20) changes depending on the NLS bound (Fig. 1(B)). The overlapping region of the N- and C-terminal arches (HEAT repeats 8-13) show no conformational change. Comparison of the four structures with the structure of the Trn1-RanGTP complex [5] demonstrates that RanGTP binding to the N-terminal arch produces substantial conformational changes in both the N- and C-terminal arches (Fig. 1(B)). The electron density appearance of the three NLSs (Fig. 1(C)) is correlated with the dissociation constant for the NLS interaction with Trn1. A NLS with a PY motif is recognized by Trn1 at two sites, Site A (HEAT repeats 8-13) with high affinity and Site B (HEAT repeats 14-18) with low affinity (Fig. 1(B)).

Figure 2(A) shows the proposed mechanism for NLS recognition and dissociation from Trn1. In the cytoplasm, Trn1 recognizes the NLS R/K/H-$X_{(2\text{-}5)}$-P-Y motif at Site A. In some cases, Trn1 changes its conformation to induce a hydrophobic interaction between Site B and the hydrophobic motif of NLS. In the nucleus, RanGTP binding to the N-terminal arch in NLS-bound Trn1 leads to a competing interaction from the H8 loop against Site B, resulting in a displacement of a NLS from Site B. After releasing from Site B, the NLS is displaced from Site A by the spatial overlap of the H8 loop with the part of the NLS at Site A. The proposed NLS dissociation model by intra-molecular interaction could be seen as a more general mechanism. For instance, the NLS dissociation from importin-α is driven by the intra-molecular interaction from the N terminal auto-inhibitory segment following dissociation of the importin-α:NLS complex from importin-β upon binding to RanGTP [6] (Fig. 2(B)). The N terminal auto-inhibitory segment of the importin-α could be functionally equivalent to the H8 loop of the Trn1.

REFERENCES

[1] E. J. Tran and S. R. Wente, *Cell,* **125** (2006) 1041.
[2] M. Iijima, M. Suzuki, A. Tanabe, A. Nishimura and M. Yamada, *FEBS Lett.*, **580** (2006) 1365.
[3] M. Suzuki, M. Iijima, A. Nishimura, Y. Tomozoe, D. Kamei and M. Yamada , *FEBS J.*, **272** (2005) 3975.
[4] T. Imasaki, T. Shimizu, H. Hashimoto, Y. Hidaka, S. Kose, N. Imamoto, M. Yamada and M. Sato, *Mol. Cell,* **28** (2007) 57.
[5] Y. M. Chook and G. Blobel, *Nature,* **399** (1999) 230.
[6] S.J. Lee, Y. Matsuura, S.M. Liu and M, Stewart, *Nature,* **435** (2005) 693.

BEAMLINE

AR-NW12A

T. Imasaki, T. Shimizu, H. Hashimoto, M. Yamada and M. Sato (Yokohama City Univ.)

Structural Analysis of a 1.1 MDa Giant Cell Surface Protein Ebh from *Staphylococcus aureus*

Staphylococcus aureus is a major cause of hospital- and community-acquired infections, and causes serious diseases, such as toxic shock syndrome and septicemia. Genome analyses revealed the presence of a 1.1 MDa giant cell surface protein, Ebh (Extracellular matrix Binding protein Homologue). The central region of Ebh contains 52 imperfect repeats of a unit consisting of 126 amino acids. Iteration of functional domains is commonly observed in cell-surface proteins; however, other proteins do not contain numbers of repeats as large as is observed in Ebh. In the present study, we investigated the effects of the repeats on the molecular properties using X-ray crystallography, circular dichroism spectrometry, and small-angle X-ray scattering. Based on the results, it is proposed that Ebh is a 320 nm rod-like molecule with some plasticity at the junctions between domains.

Staphylococcus aureus is a pathogenic bacterium which causes serious diseases, such as toxic shock syndrome and septicemia. Moreover, *S. aureus* has the notorious feature that it can easily acquire antibiotic resistance. Indeed, it has already acquired resistance to almost all available antibiotics, resulting in an increase in hospital-acquired infections. It was recently reported that the cell surface proteins are potent candidates for *S. aureus* vaccines, and thus these proteins are now being studied.

Genome analyses revealed the presence of a 1.1 MDa giant cell surface protein, Ebh (Extracellular matrix Binding protein Homologue). Ebh consists of several distinct regions, including a large central region with 52 imperfect repeats of 126 amino acid residues, which is further divided into two modules; an uncharacterized sugar binding module (S-module) and G-related albumin binding module (A-module). Iteration of functional domains is commonly observed in cell-surface proteins; however, other proteins do not contain numbers of repeats as large as is observed in Ebh. We investigated the structure of this giant molecule using X-ray crystallography, circular dichroism (CD) spectrometry, and small-angle X-ray scattering (SAXS).

The Se-SAD data set of two repeating units of Ebh (the 7th and 8th repeating units; Ebh-R7-R8) was collected up to a resolution of 2.35 Å at BL38B1, SPring-8. The crystal structure was determined using the Se-SAD method. The revealed structure showed that each repeat consists of two distinct three-helix bundles, which correspond to S- and A-modules. The two repeating units are tightly connected to each other with an angle of ca. 160° between their axes, resulting in a rod-like, dog-leg structure 120 Å in length (Fig.1A). Superposition of modules in different repeating units or other molecules in an asymmetric unit revealed that the module junctions have a certain degree of plasticity (Fig. 1B).

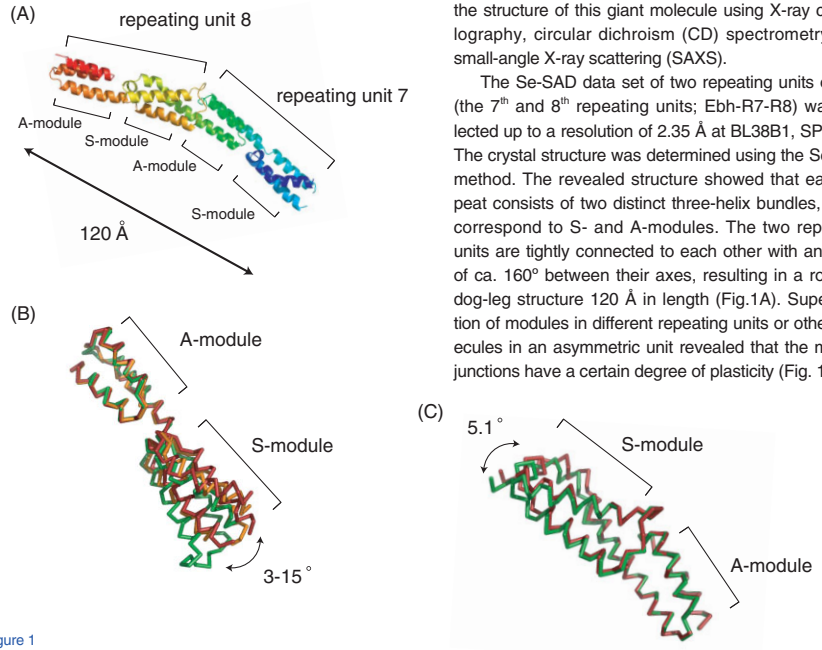

Figure 1
Crystal structure of Ebh-R7-R8.
(A) Ribbon diagram of EbhA-R7-R8. The ribbon model is colored according to the sequence, from blue at the N-terminus to red at C-terminus. The repeating units are indicated. (B) Flexibility at the junction between the S-module and the A-module. Superposition of the 7th repeating unit (red), the 8th repeating unit (green), and the 1st repeating unit determined by Cymborowski et al. (PDB code: 1xvh) (orange). The A-modules are superposed. (C) Flexibility at the junction between the A-module and S-module. Superposition of the A-module in the 7th repeating unit and the S-module in the 8th repeating unit in two molecules in an asymmetric unit. A-modules are superposed.

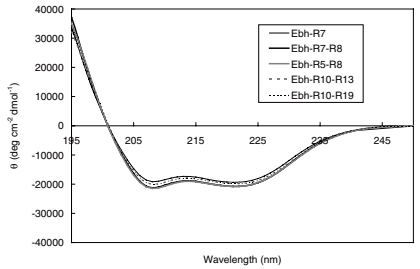

Figure 2
CD spectra of five partial proteins of Ebh

To evaluate the structure of each repeating unit in other repeating unit-linked proteins, five types of partial protein; i.e. proteins containing only the 7th repeating unit (Ebh-R7), the 7th and 8th repeating units (Ebh-R7-R8), the 5th–8th repeating units (Ebh-R5-R8), the 10th–13th repeating units (Ebh-R10-R13), and the 10th –19th repeating units of EbhA (Ebh-R10-R19) were analyzed using CD spectrometry. All the proteins showed spectra typical of an α-helical structure with two negative peaks at 208 and 222 nm, and they could be superposed well (Fig. 2). These results indicate that each repeating unit has an identical structure, and are simply iterated, with no novel structures.

To acquire an insight into the overall structure of Ebh, the low resolution structure of three partial proteins, Ebh-R7, Ebh-R7-R8, and Ebh-R5-R8, were modeled from SAXS data using an ab initio method. The SAXS data were recorded at BL10C at the Photon Factory, and the structure models were calculated using the program DAMMIN. The structures calculated for Ebh-R7 and Ebh-R7-R8 were columnar structures with length of 80 and 110 Å, respectively, which agreed well with the crystal structures (Fig. 3A and B). This indicates the applicability of ab initio modeling from SAXS data. The low resolution structure of Ebh-R5-R8 was a slightly distorted rod-like shape ca. 200 Å in length, which can be well superposed to the structure of Ebh-R5-R8 as modeled from the crystal structure of Ebh-R7-R8 by simply superposing one repeating unit onto the next (Fig. 3C). This result suggests that Ebh-R5-R8 exists as a rod-like molecule in solution, with four repeating units linearly connected.

Taken together, it is plausible that all 52 repeating units repeated in whole-length Ebh are located tandemly. The average axial translation per structural unit calculated form the crystal structure is 61.21 Å. From this value, it is proposed that Ebh has an elongated structure 320 nm in length, with some plasticity at the junctions between domains.

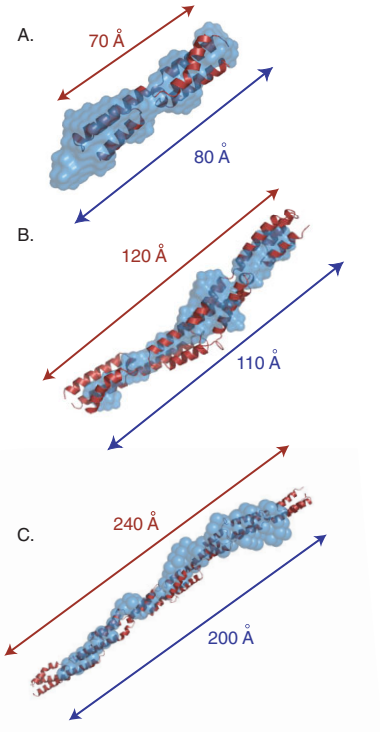

Figure 3
Low-resolution structures calculated by ab initio modeling from SAXS data.
The low-resolution structures are shown as blue balls. The crystal structures of (A) Ebh-R7 and (B) Ebh-R7-R8 are shown as red ribbon diagrams. The structure of (C) Ebh-R5-R8 as deduced from the crystal structure of Ebh-R7-R8 is also shown as a red ribbon diagram. The lengths of the structures are also indicated in blue (low resolution structures) and red (crystal structures).

REFERENCE

[1] Y. Tanaka, S. Sakamoto, M. Kuroda, S. Goda, Y.-G. Gao, K. Tsumoto, Y. Hiragi, M. Yao, N. Watanabe, T. Ohta and I. Tanaka, *Structure*, **16** (2008) 488.

BEAMLINE

10C

Y. Tanaka[1,2], S. Sakamoto[2], M. Kuroda[3], S. Goda[4], Y.G. Gao[1], K. Tsumoto[2], Y. Hiragi[5], M. Yao[1], N. Watanabe[1], T. Ohta[3], and I. Tanaka[1] ([1]Hokkaido Univ., [2]The Univ. of Tokyo, [3]Univ. of Tsukuba, [4]Nagasaki Univ., [5]Kansai Medical Univ.)